

Many-electron character of two-photon above-threshold ionization of Ar

I. D. Petrov and B. M. Lagutin

Rostov State University of Transport Communications, 344038 Rostov-on-Don, Russia

V. L. Sukhorukov and N. M. Novikovskiy

Institute of Physics, Southern Federal University, 344090 Rostov-on-Don, Russia

Ph. V. Demekhin, A. Knie, and A. Ehresmann

*Institute of Physics and Center for Interdisciplinary Nanostructure Science and Technology (CINSaT),
University Kassel, D-34132 Kassel, Germany*

(Received 8 October 2018; published 9 January 2019)

The absolute generalized cross sections and angular distribution parameters of photoelectrons for the two-photon above-threshold $3p$ ionization of Ar were calculated in the exciting photon energy range from 15.76 to 36 eV. The correlation function technique developed earlier was extended for the case when an intermediate-state function is of a continuum-type. We show that two-photon ionization of Ar near the $3p^4$ threshold to a large extent is determined by the $(3p \rightarrow \epsilon d)^2$ two-photon absorption via the giant resonance. This many-electron correlation causes (i) an increase of the photoionization cross sections by more than a factor of 3; and (ii) the appearance of resonances in the exciting-photon energy range of the doubly excited states. The predictions are supported by a good agreement between length and velocity results obtained after taking into account the higher-order perturbation theory corrections.

DOI: [10.1103/PhysRevA.99.013408](https://doi.org/10.1103/PhysRevA.99.013408)**I. INTRODUCTION**

Advancements in new intense and tunable free-electron lasers (FELs) [1–5] covering the ultraviolet and x-ray photon-energy ranges inspire a renewed interest for a detailed comprehension of multiphoton processes. Experimental data obtained using FELs are of great motivation for theory to provide not only a qualitative but also a quantitative description of new phenomena.

One of these cases is atomic two-photon above-threshold ionization (ATI) when the energy of a single photon is sufficient to ionize an atom. It has been shown [6–11] that below the one-photon ionization threshold, many-electron correlations significantly influence the calculated cross sections and angular distribution parameters of photoelectrons with respect to those obtained in a single-electron approximation. The intermediate-state shake-up correlation studied in [9–11] resulted in a noticeably closer agreement of the generalized two-photon ionization cross section (G2PICS) calculated in length (G2PICS- L) and velocity (G2PICS- V) forms of the electric dipole operator. The final-state electron scattering correlations taken into account in [7–11] decrease noticeably the absolute values of G2PICS. In contrast, the polarization of the atomic core by the photoelectron [10,11] increases the cross sections by 15–20 %.

To the best of our knowledge, there is only one *ab initio* theoretical description of the two-photon ATI of Ar [12]. Those calculations were carried out using Herman-Skillman [13] potential for computing atomic orbitals (AOs) without considering the collective behavior of electrons.

In this work, we intend to take into account many-electron correlations in the calculation of the $3p$ -ATI of Ar. To solve

this problem, the correlation function (CF) technique developed by us in [10,11] for the exciting-photon energy region below the one-photon ionization threshold is applied. We extend the CF technique for the ATI case solving two challenging problems: (i) computing the CFs for positive energy, i.e., in the continuum, satisfying the correct boundary conditions; and (ii) computing the free-free dipole transition matrix elements containing the CF and final-state wave function, both of continuum-type.

The paper is organized as follows. In Sec. II we describe the correlation function method for a two-photon transition amplitude calculation in the above-threshold exciting-photon energy region. The technique of the matrix element calculation for the two continuum-state functions is also described in detail. In Sec. III the developed method is applied to the calculation of partial and total G2PICS of the $3p$ shell of Ar above the $3p$ threshold. Various correlation effects are considered and discussed. The influence of many-electron correlations on the angular-distribution parameters of the photoelectrons is studied in Sec. IV. We conclude with a brief summary in Sec. V.

II. TWO-PHOTON TRANSITION AMPLITUDES FOR THE ABOVE-THRESHOLD PHOTON ENERGIES

To investigate the influence of many-electron correlations on the ATI of atoms, we considered the two-photon $3p$ ionization of argon applying the LS -coupling scheme:

$$\text{Ar } 3p^6(^1S) + 2\gamma \rightarrow \text{Ar } 3p^5(^2P)\epsilon\ell(^1L) \quad (L = 0; 2). \quad (1)$$

Here L and ℓ are the orbital angular momenta of the final state and photoelectron, respectively. We investigate the case when the energy of a single photon is sufficient to ionize the atom. This process is known as above-threshold ionization (ATI).

The amplitude of the two-photon ionization transition $i \rightarrow f$ with photon energy ω in the lowest order of perturbation theory (LOPT) in the ATI energy region is given by

$$T_{i \rightarrow f} = \sum_m \frac{\langle f | D | m \rangle \langle m | D | i \rangle}{E_i + \omega - E_m + i\delta}, \quad \delta \rightarrow 0+, \quad (2)$$

where E_i and E_m are energies of the initial and intermediate states, respectively, D is the electric dipole operator, δ is an infinitesimal positive quantity, and the sum contains all possible intermediate states m including continuum ones. The contributions accounting for many-electron correlations were taken into account in addition to the LOPT amplitude (2). We study all possible correlations that are allowed in the next order of perturbation theory due to Coulomb interaction of electrons. These transitions can schematically be presented as shown below.

The LOPT processes are

$$p^6 \dashrightarrow p^5 \varepsilon' \ell' \dashrightarrow p^5 \varepsilon \ell, \quad (\text{Ia})$$

$$s^2 p^6 \dashrightarrow s^1 p^6 \varepsilon \ell \dashrightarrow s^2 p^5 \varepsilon \ell. \quad (\text{Ib})$$

Here and below, the dashed arrows denote electric dipole interaction and solid arrows denote Coulomb interaction of electrons.

The correlations described by the next order of perturbation theory are classified as follows:

Intermediate-state interchannel correlation:

$$p^6 \dashrightarrow p^5 \varepsilon'' \ell'' \rightarrow p^5 \varepsilon' \ell' \dashrightarrow p^5 \varepsilon \ell. \quad (\text{II})$$

Ground-state correlations:

$$p^6 \rightarrow p^4 \varepsilon' \ell' \varepsilon'' \ell'' \dashrightarrow p^5 \varepsilon' \ell' \dashrightarrow p^5 \varepsilon \ell, \quad (\text{IIIa})$$

$$p^6 \rightarrow p^4 \varepsilon' \ell' \varepsilon'' \ell'' \dashrightarrow p^4 \varepsilon \ell \varepsilon'' \ell'' \dashrightarrow p^5 \varepsilon \ell, \quad (\text{IIIb})$$

$$p^6 \rightarrow p^4 \varepsilon \ell \varepsilon'' \ell'' \dashrightarrow p^4 \varepsilon \ell \varepsilon' \ell' \dashrightarrow p^5 \varepsilon \ell. \quad (\text{IIIc})$$

Intermediate-state shake-up correlation:

$$p^6 \dashrightarrow p^5 \varepsilon' \ell' \rightarrow p^4 \varepsilon \ell \varepsilon' \ell' \dashrightarrow p^5 \varepsilon \ell. \quad (\text{IV})$$

Intermediate-state electron-scattering correlations:

$$p^6 \dashrightarrow p^5 \varepsilon' \ell' \rightarrow p^4 \varepsilon \ell \varepsilon'' \ell'' \dashrightarrow p^5 \varepsilon \ell. \quad (\text{V})$$

Final-state electron-scattering correlations:

$$p^6 \dashrightarrow p^5 \varepsilon' \ell' \dashrightarrow p^4 \varepsilon' \ell' \varepsilon'' \ell'' \rightarrow p^5 \varepsilon \ell, \quad (\text{VIa})$$

$$p^6 \dashrightarrow p^5 \varepsilon'' \ell'' \dashrightarrow p^4 \varepsilon' \ell' \varepsilon'' \ell'' \rightarrow p^5 \varepsilon \ell. \quad (\text{VIb})$$

A. Correlation function for positive energy

The radial part of the amplitude for process (Ia) is

$$t_{\omega}^{(\text{Ia})}(L, \ell, \ell') = \sum_{\varepsilon' > F} \frac{\langle \varepsilon \ell | d_r | \varepsilon' \ell' \rangle \langle \varepsilon' \ell' | d_r | 3p \rangle}{\omega - E_{3p}^{(i)} - \varepsilon' + i\delta}, \quad (3)$$

where $E_{3p}^{(i)}$ is the ionization potential of the $3p$ electron in Ar, d_r is the radial part of the dipole transition operator obtained

in the length or velocity form, and the notation $\varepsilon' > F$ denotes the summation over all unoccupied single-electron states. The wave function of the photoelectron, $|\varepsilon \ell\rangle$, depends on the orbital momentum L of the final state.

The infinite summation in (3) can be efficiently performed by the correlation-function (CF) method ([10,11] and references therein). In the ATI case, the CF should satisfy the outgoing-wave boundary conditions, and it is a solution of the inhomogeneous integrodifferential equation

$$(h_{\ell'} - \omega + E_{3p}^{(i)})\phi_{\ell'}(r) = -d_r P_{3p}(r) + \sum_{n' < F} P_{n'\ell'}(r) \times \langle n' \ell' | d_r | 3p \rangle, \quad (4)$$

where $h_{\ell'}$ is the Hartree-Fock operator for the $\varepsilon' \ell'$ function in the configuration $3p^5 \varepsilon' \ell' ({}^1P)$.

To obtain the continuum-type CF, we have used a technique similar to that presented in [14]. First, the inhomogeneous equation (4) is solved disregarding the boundary conditions at large distances ($r \rightarrow \infty$). This solution, which we denote $\Lambda_{\ell'}$, has a nonzero contribution from the incoming waves, and its asymptotic behavior at ($r \rightarrow \infty$) can be expressed as

$$\Lambda_{\ell'}(r) = gG(r) + hH(r), \quad (5)$$

where $G(r)$ and $H(r)$ are regular and irregular Coulomb functions, respectively [15], asymptotically denoted as

$$G_{\varepsilon \ell}(r) \xrightarrow{r \rightarrow \infty} \sqrt{\frac{2}{\pi k}} \sin \left(kr - \frac{\ell\pi}{2} + \frac{Z}{k} \ln(2kr) + \delta_{\ell} \right), \quad (6)$$

$$H_{\varepsilon \ell}(r) \xrightarrow{r \rightarrow \infty} -\sqrt{\frac{2}{\pi k}} \cos \left(kr - \frac{\ell\pi}{2} + \frac{Z}{k} \ln(2kr) + \delta_{\ell} \right). \quad (7)$$

Here, k is the wave vector of the continuum electron in atomic units, Z is the asymptotic charge of the ionic core, and δ_{ℓ} represents the sum

$$\delta_{\ell} = \arg \Gamma \left(\ell + 1 - i \frac{Z}{k} \right) + \varphi_{\ell}, \quad (8)$$

where φ_{ℓ} is the short-range phase shift. Coefficients g and h in (5) are defined by matching the respective numerical solutions of inhomogeneous Eq. (4) starting upward from zero and downward from infinity.

To obtain the solution of Eq. (4), which has the correct boundary condition appropriate for the photoionization case, we add the general solution $P_{\varepsilon' \ell'}(r)$ of the homogeneous equation to $\Lambda_{\ell'}(r)$, factorized with a coefficient A ,

$$(h_{\ell'} - \omega + E_{3p}^{(i)})P_{\varepsilon' \ell'}(r) = 0. \quad (9)$$

The solution of Eq. (4), which has the correct boundary conditions, is thus given by

$$\phi_{\ell'}(r) = \Lambda_{\ell'}(r) + A P_{\varepsilon' \ell'}(r), \quad (10)$$

where $\Lambda_{\ell'}(r)$ is the solution (5) of Eq. (4) with unphysical boundary conditions.

The solution of the homogeneous equation (9) in its asymptotics ($r \rightarrow \infty$) can be determined as

$$P_{\varepsilon' \ell'}(r) = G(r) - K H(r), \quad (11)$$

where the coefficient K is obtained by matching the respective numerical solutions of Eq. (9) starting upward from zero and downward from infinity.

Substituting Eqs. (5) and (11) into (10), applying the Euler expressions $\sin x = \frac{i}{2}(e^{-ix} - e^{ix})$ and $\cos x = \frac{1}{2}(e^{-ix} + e^{ix})$ with $x = kr - \frac{\ell\pi}{2} + \frac{Z}{k}\ln(2kr) + \delta_\ell$, and equating a factor at e^{-ix} to zero, we obtain the following formulas for the coefficient A in Eq. (10):

$$\operatorname{Re}A = -\frac{hK + g}{K^2 + 1}, \quad \operatorname{Im}A = \frac{gK - h}{K^2 + 1}. \quad (12)$$

After the CF is determined in the form of (10), the radial part of the transition amplitude (3) takes the following form:

$$t_{q,\omega}^{(1a)}(L, \ell, \ell') = \langle \varepsilon \ell | d_r | \phi_{\ell'} \rangle. \quad (13)$$

B. Calculation of the electric dipole transition amplitude between two continuum-type functions

In Eq. (13) both the CF, $\phi_{\ell'}(r)$, and the final-state AO, $P_{\varepsilon\ell}(r)$, are of continuum-type. To calculate the dipole integral (13) between the two continuum wave functions, a special technique was applied. We used the method described in [16,17]. According to this method, the dipole integral (13) is expressed as

$$\langle \varepsilon \ell | d_r | \phi_{\ell'} \rangle = \int_0^{r_0} P_{\varepsilon\ell}(r) dr \phi_{\ell'}(r) + I(r_0, \varepsilon\ell, \varepsilon'\ell'), \quad (14)$$

where r_0 is a sufficiently large value of r and

$$I(r_0, \varepsilon\ell, \varepsilon'\ell') = \int_{r_0}^{\infty} u_{\varepsilon\ell}(r) dr u_{\varepsilon'\ell'}(r). \quad (15)$$

The radial functions $u_{\varepsilon\ell}(r)$ in (15) are the standard Coulomb functions, which are the solutions of the equation

$$\left(\frac{d^2}{dr^2} + f_\ell(r) \right) u_{\varepsilon\ell}(r) = 0, \quad (16)$$

$$f_\ell(r) = k^2 + \frac{2Z}{r} - \frac{\ell(\ell+1)}{r^2} \quad (r \geq r_0),$$

where $\varepsilon(\text{Ry}) = k^2$.

The solutions of Eq. (16) are asymptotically expressed as

$$u_{\varepsilon\ell}(r) = \sqrt{\frac{2}{\pi \xi_\ell(r)}} \sin(\Phi_\ell^{(1)}(r) + \delta_\ell). \quad (17)$$

In Eq. (17), an approximate value of $\Phi_\ell^{(1)}(r)$ with an accuracy of $1/r^4$ can be obtained using the formulas presented in [18,19]:

$$\begin{aligned} \Phi_\ell^{(1)} = & x + \frac{1}{m} \ln \left(\frac{1}{m} + m\rho + x \right) - \frac{1}{m} - \frac{\ell\pi}{2} \\ & + y - \frac{x(3m^2t + 4) + m\rho(3m^2t + 2) + mt}{24(1 + m^2t)x(x + m\rho)} \\ & + \frac{5(\rho - t)}{24x^3}, \end{aligned} \quad (18)$$

where the abbreviations $m = k/Z$, $\rho = Zr$, $x = (m^2\rho^2 + 2\rho - t)^{1/2}$, $t = \ell(\ell + 1)$, and

$$y = \begin{cases} \frac{t+1/8}{\sqrt{t}} \arccos \left[\frac{\rho-t+mtx}{(1+m^2t)\rho} \right], & l > 0; \\ \frac{1}{4(x+m\rho)}, & l = 0. \end{cases} \quad (19)$$

are used. Note that there is a ‘‘sign’’ misprint in the definition of x in Eq. (19.44) of Ref. [18], whereas Eq. (16) of Ref. [19] contains a misprint corrected in the present Eq. (18).

The amplitude function $\xi_\ell(r)$ appearing in Eq. (17) satisfies the following differential equation:

$$\xi_\ell^2(r) = f_\ell(r) + \xi_\ell^{1/2}(r) \frac{d^2}{dr^2} \xi_\ell^{-1/2}(r). \quad (20)$$

Equation (20) can be solved iteratively. A zeroth approximation is expressed as $\xi_\ell^{(0)}(r) = \sqrt{f_\ell}$. The next approximation can be calculated by [18]

$$\xi_\ell^{(1)} = \sqrt{f_\ell + \xi_\ell^{1/4} \frac{d^2}{dr^2} \xi_\ell^{-1/4}} = \sqrt{f_\ell + \frac{5}{16} \left(\frac{f'_\ell}{f_\ell} \right)^2 - \frac{1}{4} \frac{f''_\ell}{f_\ell}}. \quad (21)$$

Integral (15) can be expressed as a difference of two terms:

$$I(r_0, \varepsilon\ell, \varepsilon'\ell') = I^+ - I^-, \quad (22)$$

where

$$I^\pm = \lim_{\varepsilon \rightarrow 0} \int_{r_0}^{\infty} e^{-\varepsilon r} \xi^\pm(r) g^\pm(r) \cos \chi^\pm(r) dr, \quad (23)$$

$$\xi^\pm(r) = \xi_{\ell'}^{(1)}(r) \pm \xi_\ell^{(1)}(r), \quad (24)$$

$$g^\pm(r) = d_r \left[\pi \left(\xi_{\ell'}^{(1)} \xi_\ell^{(1)} \right)^{1/2} \xi^\pm \right]^{-1}, \quad (25)$$

$$\chi^\pm(r) = [\Phi_{\ell'}^{(1)} + \delta_{\ell'}] \pm [\Phi_\ell^{(1)} + \delta_\ell]. \quad (26)$$

After subsequent integration of Eq. (23) by parts, the following expansion can be obtained [17]:

$$I^\pm = \left\{ \sum_{n=0}^{\infty} \left[\left(\frac{1}{\xi^\pm} \frac{d}{dr} \right)^n g^\pm(r) \right] \sin \left(\chi^\pm(r) + \frac{n\pi}{2} \right) \right\}_{r=r_0}. \quad (27)$$

In the present calculation, we included the first four terms of expansion (27).

C. Additional computational remarks

The wave functions of the atomic core of Ar were computed on the ground-state configuration $1s^2 2s^2 2p^6 3s^2 3p^6$ obtained in the Hartree-Fock (HF) approximation. The final-state wave functions were obtained by solving the HF equations for a photoelectron in the configurations $3p^5 \varepsilon p(^1S)$, $3p^5 \varepsilon p(^1D)$, and $3p^5 \varepsilon f(^1D)$ using frozen core functions. The same frozen core functions were used in the $h_{\ell'}$ operator in Eq. (4).

The Hartree-Fock operator entering Eq. (4) includes the nonlocal exchange part of the Coulomb interaction of the CF with core electrons. In the same way as in [10], a separate local differential equation is determined for each term of the exchange Coulomb potential. As a result, the single

nonlocal integrodifferential equation (4) is transformed to a system of local differential equations. To solve this system, a noniterative numerical procedure is applied that is stable and converges at each energy.

The calculation of the transition amplitude (Ib) via the $3s$ shell is identical for above (ATI) and below threshold ionization. The latter case has been described in our previous work [10]. The correlation transition amplitudes (II)–(V) were calculated using the CF technique. The respective inhomogeneous equations were presented and discussed in [10]. In the ATI energy region, the calculations of the CFs are different in two cases. First, if the energy denominator in the expression for the transition amplitude has no pole, then the corresponding CF is of discrete-type, consists of a real part only, and is calculated using the technique from Ref. [10]. Second, if the energy denominator has a pole, then the CF is of continuum-type, consists of real and imaginary parts, and is computed using the method described above.

III. GENERALIZED TWO-PHOTON IONIZATION CROSS SECTION FOR ABOVE-THRESHOLD IONIZATION OF THE $3p$ SHELL OF AR

To characterize two-photon ionization quantitatively, we use the generalized two-photon ionization cross section (G2PICS) as defined in [7,9,10]. This intrinsic quantity does not contain the exciting-photon flux and is therefore ideally suited to characterize this process. The expression for the G2PICS is

$$\sigma_q(\omega) = \sum_{L,\ell} \sigma_q(L, \ell, \omega), \quad (28)$$

where $q = 0$ and ± 1 correspond to a linearly or circularly polarized incoming radiation, respectively. Each partial generalized cross section is determined in $\text{cm}^4 \text{s}$ and expressed via the two-photon transition amplitudes $T_{q,\omega}(L, \ell)$ [10] as

$$\sigma_q(L, \ell, \omega) = \frac{8\pi^3 \alpha a_0^5}{c} \omega^{\pm 2} |T_{q,\omega}(L, \ell)|^2. \quad (29)$$

In Eq. (29), $\alpha = 1/137.036$ is the fine-structure constant, $a_0 = 5.29177 \times 10^{-9} \text{ cm}$ is the Bohr radius, $c = 2.99792 \times 10^{10} \text{ cm/s}$ is the light velocity in vacuum, and ω is the exciting photon energy in atomic units; $+$ and $-$ correspond to the length and velocity form of the electric dipole transition operator. The major details of the transition amplitude calculation (particularly the calculation of the angular parts) have been described in our previous work [10].

A. LOPT approximation

The G2PICS of the $3p$ shell of Ar calculated in the LOPT approximation [processes (Ia) and (Ib)] are presented in Fig. 1 in the exciting-photon energy region below the one-photon ionization threshold (our calculation from [10]) and in the ATI region (the present calculation). In the same figure, the results of the G2PICS of Ar computed in [12] in the LOPT approach are also depicted.

The total G2PICS have been plotted in [12] versus the energy $\varepsilon_1 = -|\varepsilon_{3p}| + \omega$ of the electron in the intermediate state. In our calculation, the G2PICS are presented as functions of

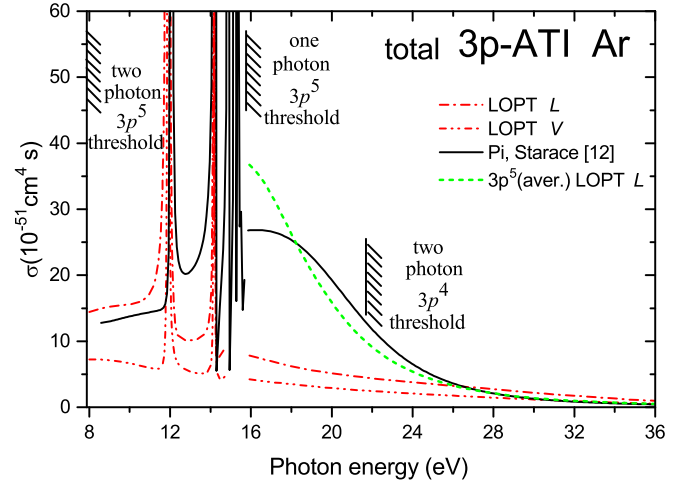


FIG. 1. The $3p$ shell total G2PICS in length (L) and velocity (V) form for linearly polarized incoming radiation calculated in LOPT below the one-photon $3p$ threshold [10] and in the ATI region (present work). The calculation of [12] and the data obtained in the average $3p^5$ relaxed core are also presented for comparison (see text). The two-photon $3p^5(^2P_{3/2})$ and $3p^4(^3P_2)$ thresholds and one-photon $3p^5(^2P_{3/2})$ threshold from [20] are depicted as hatched lines.

the exciting-photon energy ω . To compare our data with the data of [12], we used the experimental one-photon ionization potential of the $3p$ -electron $E_{3p}^{(i)} = 1.158 \text{ Ry}$ [corresponding to the energy level $E(^2P_{3/2}) = 15.7596 \text{ eV}$ [20]] instead of the Herman-Skillman value $|\varepsilon_{3p}| = 1.065 \text{ Ry}$ used in [12]. This aligns the one-photon ionization thresholds in both calculations (see the hatched line at 15.76 eV in Fig. 1).

The G2PICS obtained in [12] agree fairly well with our calculation close to the two-photon ionization threshold ($\omega = 7.8798 \text{ eV}$). The data of [12] are located between our G2PICS- L and G2PICS- V and differ from our G2PICS- L by 15%. The deviation is larger in the ATI region, as seen from Fig. 1. At the one-photon $3p^5$ threshold, the cross section from [12] exceeds our G2PICS- L by more than three times, whereas at high photon energies it decreases more rapidly than our G2PICS, and after $\omega = 30 \text{ eV}$ it is close to the present G2PICS- V . We suggest that this disagreement arises most likely from the different approximations in the CFs calculation: Herman-Skillman in [12] versus term-dependent Hartree-Fock $3p^5\phi_{\ell'}(^1P)$ in the present work.

To support this suggestion, we performed a separate study by calculating the G2PICS in the LOPT approach using the average self-consistent $3p^5\varepsilon'\ell'$ configuration instead of the term-dependent frozen core $3p^5\varepsilon'\ell'(^1P)$ configuration. We choose the relaxed $3p^5$ core because calculation performed within this approach yields the single-photon $3p$ -photoionization cross section of Ar close to the Herman-Skillman result. The two-photon G2PICS- L calculated in the relaxed $3p^5$ core presented in Fig. 1 became closer to those obtained in [12], which supports our assumption.

The value of amplitude (Ib) for the transition via the $3s$ shell is less than 0.1% of the amplitude (Ia) and has practically no influence on the calculated cross section.

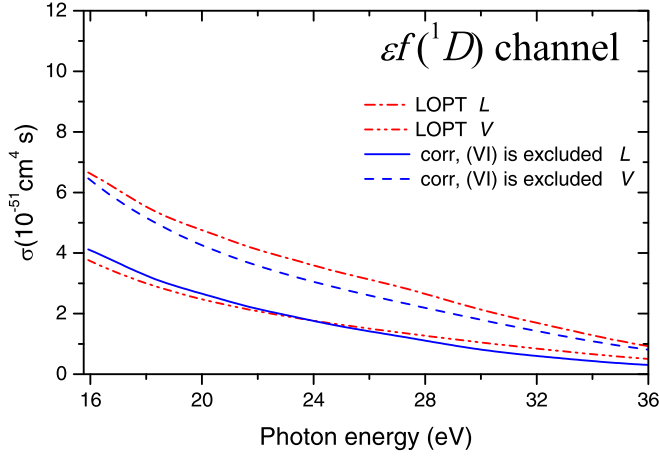


FIG. 2. Partial G2PICS for the transition to the $3p^5\epsilon f(^1D)$ channel, computed in length (L) and velocity (V) form for linearly polarized incoming radiation in LOPT and with accounting for transitions (I)–(V) [corr (VI) is excluded].

The results depicted in Fig. 1 show that the G2PICS calculated in our work in the LOPT approximation in the length and velocity forms differ from each other by approximately two times. This difference indicates the necessity to include many-electron correlation in the calculation.

B. Correlation processes of third order of perturbation theory

The total two-photon ionization cross section of the $3p$ shell of Ar is a sum of three partial cross sections for the

$$t_{\omega}^{(VIa,b)}(L, \ell, \ell', \ell'') = \sum_{\ell', \ell'' > F} \sum_k [a_k R^k(\epsilon \ell 3p, \ell' \ell' \ell'') + b_k R^k(\epsilon \ell 3p, \ell'' \ell'' \ell' \ell')] \langle \ell'' \ell'' | d_r | 3p \rangle \langle \ell' \ell' | d_r | 3p \rangle \times \left\{ \frac{1}{(2\omega - E_{3p^2}^{(i)} - \epsilon' - \epsilon'')(\omega - E_{3p}^{(i)} - \epsilon')} + \frac{1}{(2\omega - E_{3p^2}^{(i)} - \epsilon' - \epsilon'')(\omega - E_{3p}^{(i)} - \epsilon'')} \right\}, \quad (30)$$

where $E_{3p^2}^{(i)} = 3.189$ Ry is the experimental 43.3893 eV [20] energy of the $3p^4(^3P_2)$ level. The a_k and b_k are numerical coefficients given in [10], and $R^k(\epsilon \ell 3p, \ell' \ell' \ell'')$ is the Slater integral

$$R^k(n_1 \ell_1, n_3 \ell_3; n_2 \ell_2, n_4 \ell_4) = \int_0^{\infty} P_{n_3 \ell_3}(r) P_{n_4 \ell_4}(r) y_k(P_{n_1 \ell_1}, P_{n_2 \ell_2}; r) dr, \quad (31)$$

$$y_k(P_{n_1 \ell_1}, P_{n_2 \ell_2}; r) = \int_0^{\infty} \frac{r_{<}^k}{r_{>}^{k+1}} P_{n_1 \ell_1}(r') P_{n_2 \ell_2}(r') dr', \quad (32)$$

where $r_{<}$ and $r_{>}$ are the smaller and the larger of the radial coordinates r and r' .

Since the first factor in the denominator of the two terms in the curly brackets of Eq. (30) contains both the ϵ' and ϵ'' intermediate state energies, the amplitude (30) cannot be expressed via CFs. Therefore, we performed the calculation using expression (30) without any additional approximations. This was possible because in Eq. (30) both the Slater integrals $R^k(\epsilon \ell 3p, \ell'' \ell'' \ell' \ell')$ and the dipole integrals $\langle \ell' \ell' | d_r | 3p \rangle$ and $\langle \ell'' \ell'' | d_r | 3p \rangle$ are not divergent due to the presence of a localized $3p$ function. To perform the summation in Eq. (30) over

transitions to the $\epsilon p(^1S)$, $\epsilon p(^1D)$, and $\epsilon f(^1D)$ channels. As in [12], the $\epsilon f(^1D)$ channel is found to dominate in the ATI region: in the LOPT approximation at the one-photon $3p^5$ threshold, the partial $\epsilon f(^1D)$ cross sections are about 85% and 89% of the total $3p$ cross sections in the length and velocity gauge, respectively. Therefore, the influence of many-electron correlations will be demonstrated here in detail for the case of the $\epsilon f(^1D)$ channel only.

In Fig. 2, the partial G2PICS for the $\epsilon f(^1D)$ channel calculated in LOPT are compared with the cross section computed with accounting for the processes (I)–(V) [correlation (VI) is excluded]. The starting value of the photon energy corresponds to the one-photon $3p^5$ -ionization threshold $\omega = 15.7596$ eV. In Fig. 2, it is seen that the correlative transitions (II)–(V) change the G2PICS only quantitatively but without any qualitative change in their energy dependence.

It turned out that in $3p$ -ATI, correlation correction (VI) is much more important than below the one-photon $3p$ threshold. In ATI, the transition amplitude (VI) is substantially (one order of magnitude) larger than the other correlation amplitudes (II)–(V) and changes the computed cross sections drastically. In the processes (VIa) and (VIb), the first and the second photon excite a pair of $3p$ core electrons to virtual $\epsilon' \ell'$ and $\epsilon'' \ell''$ states; then because of the Coulomb interaction, one electron returns to the core and another changes the state to the $\epsilon \ell$ final one. The large value of this correlation can be explained through the existence of the giant resonance in each of the single-electron $\langle \epsilon d | d_r | 3p \rangle$ transition amplitudes.

The radial part of the transition amplitude (VI) is described by the following expression:

the $\epsilon' \ell'$ and $\epsilon'' \ell''$, several discrete states and the continuum states up to 20 Ry were taken into account.

In Fig. 3, partial GSPICS for the transition to the $3p^5\epsilon f(^1D)$ channel calculated considering the correlations (II)–(V) only and with all correlations (II)–(VI) are compared. A drastic difference between the two results is evident: (i) the G2PICS in length form is enhanced by an order of magnitude, resulting in a pronounced maximum at $\omega = 32$ eV; (ii) the correlation (VI) gives rise to doubly excited state resonances below the two-photon $3p^4$ double-ionization threshold. The resonances become apparent at those photon energies when

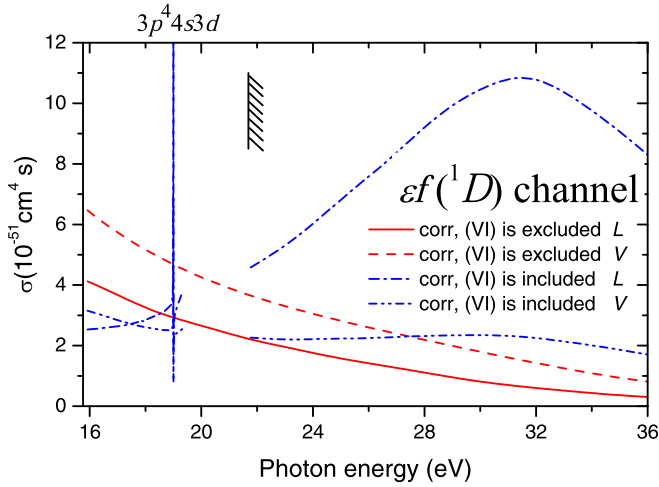


FIG. 3. Partial G2PICS for the transition to the $3p^5\epsilon f(^1D)$ channel, computed in length (L) and velocity (V) form for linearly polarized incoming radiation with accounting for transitions (I)–(V) [corr (VI) is excluded] and with accounting for all correlations (I)–(VI) [corr (VI) is included]. The two-photon $3p^4(^3P_2)$ ionization threshold is indicated by the hatched line. We show the energetically lowest calculated $3p^44s3d$ doubly excited state resonance only.

the denominators in Eq. (30) containing 2ω are vanishing. The first, energetically lowest $3p^43d4s$ resonance in the partial $3p^5\epsilon f(^1D)$ G2PICS is shown in Fig. 3. In both cross sections, G2PICS- L and G2PICS- V , this resonance is located at the same energy and has an identical narrow shape. Therefore, the profiles are overlapped and are not resolved in Fig. 3. We restricted our presentation to this resonance because the precise calculation of the doubly excited state energies is a cumbersome problem on its own (see, e.g., [21–23]). The energies of the respective doubly excited state resonances are expected to be larger than they appear in the relaxed $3p^4n'\ell'n''\ell''$ configuration. The two-photon double-ionization threshold equal to $0.5E_{3p_2}^{(i)}$ is depicted in Fig. 3 by the hatched line. It indicates the upper limit of the doubly excited state resonances.

The revealed strong influence of many electron correlations on G2PICS including the resonance structure is beyond a simple single-electron picture of two-photon ionization, and its experimental verification is of great fundamental importance.

C. Many-electron correlations of higher orders of perturbation theory

G2PICS calculated in length and velocity gauges considering all the transitions (I)–(VI) still differ substantially, as is seen from Fig. 3. At $\omega = 32$ eV the G2PICS- L (dashed-dotted line) is four times larger than G2PICS- V (dash-double-dotted line). In our work [10], a good agreement between computed G2PICS- L and G2PICS- V was achieved after inclusions of higher-order PT correlations. Those effects were (i) the polarization of the atomic core by the photoelectron, and (ii) the correlational decrease of the Coulomb interaction in the description of the correlative processes (II)–(VI). Additional calculations showed that in the ATI region, taking into account these higher-order PT correlations, (i)–(ii) is

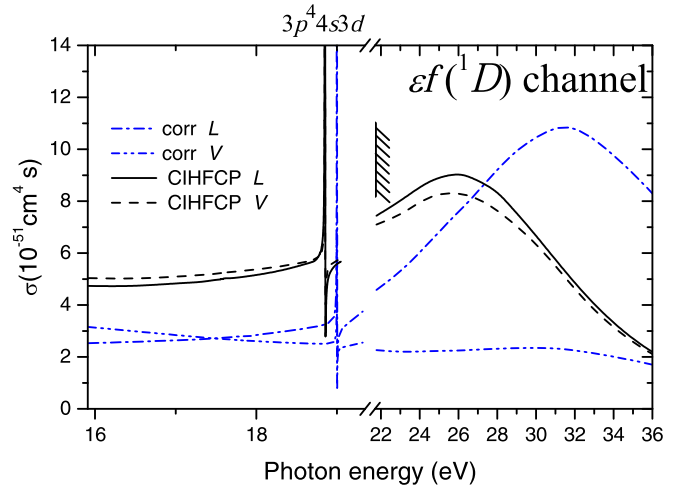


FIG. 4. Partial G2PICS for the transition to the $3p^5\epsilon f(^1D)$ channel, computed in length (L) and velocity (V) form for linearly polarized incoming radiation with accounting for all the correlations (I)–(VI) (corr) and, in addition, the higher-order PT correlations (CIHFPC). The two-photon $3p^4(^3P_2)$ ionization threshold is indicated by the hatched line. The first calculated $3p^44s3d$ doubly excited state resonance is shown only.

not sufficient to make an agreement between G2PICS- L and G2PICS- V close. The reason is the anomalously large contribution of the correlation (VI) discussed above. In the present work, we take into account intrashell correlations [24] in addition to correlations (i)–(ii) when computing the matrix elements $\langle \epsilon'\ell'|d_r|3p \rangle$ and $\langle \epsilon''\ell''|d_r|3p \rangle$.

The *ab initio* core polarization potential $V^{\text{CP}}(r)$ [25] was included in the HF operator $h_{\ell}(r)$ entering the equations for the CFs and for the final-state electrons. In addition, the matrix elements of the Coulomb interaction describing the correlations (II)–(VI) have been reduced by a factor of 1.25 [10]. Here and below, the calculation with taking into account the processes (I)–(VI), intrashell correlations, polarization of the atomic core by the photoelectron, and the correlational decrease of the Coulomb interaction will be designated as the configuration interaction Hartree-Fock approach with core polarization (CIHFPC).

The CIHFPC partial cross sections for the $\epsilon f(^1D)$ channel are depicted in Fig. 4 (solid and dashed curves for length and velocity form, respectively). In the same figure, the cross sections calculated with taking into account processes (I)–(VI) but without higher-order PT corrections are also presented (dash-dotted and dash-double-dotted curves) for comparison. It is clearly seen that accounting for higher-order PT corrections results in a very close agreement between the G2PICS- L and G2PICS- V both above the two-photon double-ionization threshold (to the right of the hatched line in Fig. 4) and in the region of the $3p^44s3d$ resonance. The following changes in the calculated G2PICS can be seen from Fig. 4:

(i) The energy of the $3p^44s3d$ resonance shifted by 0.15 eV to the low-energy side. The reason for the shift is the polarization of the atomic core by the photoelectron, which decreases energies of the excited electrons.

(ii) The polarization potential attracts the photoelectron AOs to smaller distances (see also Fig. 1 in [26]), which

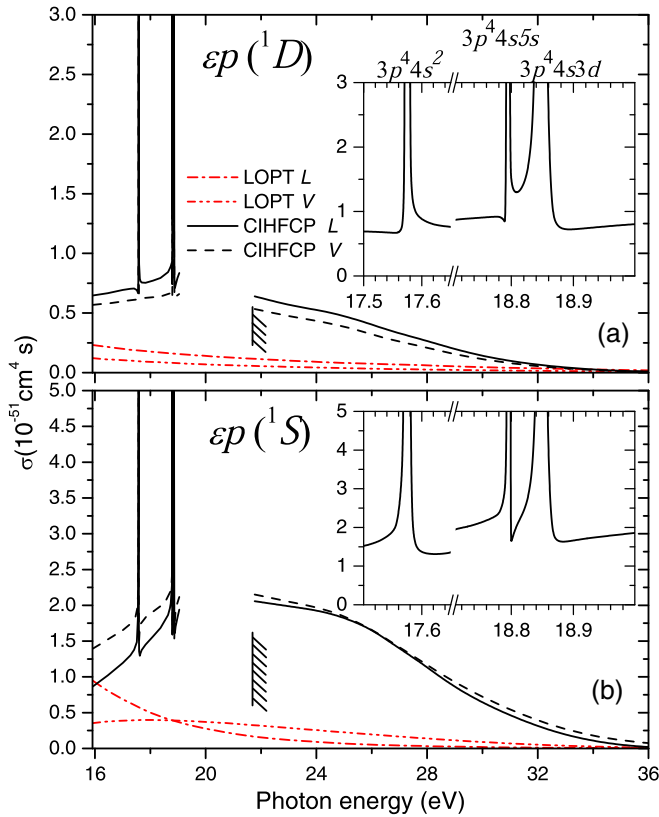


FIG. 5. Partial G2PICS for the transitions to the $3p^5\epsilon p(^1D)$ channel (a) and to the $3p^5\epsilon p(^1S)$ channel (b), computed in length (L) and velocity (V) form for linearly polarized incoming radiation in LOPT and with taking into account both the correlations (I)–(VI) and higher-order PT correlations (CIHFPC). The two-photon $3p^4(^3P_2)$ ionization threshold is indicated by the hatched line.

causes the G2PICS to increase on the one-photon threshold ($\omega = 15.76$ eV) by about two times and shifts the maximum in the $\sigma(\omega)$ dependence above the two-photon $3p^4$ threshold by ~ 6 eV to the low-energy side.

The computed partial G2PICSs for the transitions to the $3p^5\epsilon p(^1D)$ and $3p^5\epsilon p(^1S)$ channels are depicted in Figs. 5(a) and 5(b), respectively. Dash-dotted and dash-double-dotted lines represent results computed in the LOPT, and solid and dashed lines represent CIHFPC results. Similar to the $3p^5\epsilon f(^1D)$ channel, one can recognize a strong increase the G2PICSs, the appearance of the doubly excited state resonances, and a better agreement between length and velocity results.

In the insets of Figs. 5(a) and 5(b), the doubly excited state resonance region of the G2PICS-L is presented on an enlarged scale. For the $3p^5\epsilon f(^1D)$ channel, the lowest resonance corresponds to the $3p^4 4s 3d$ state (see Figs. 3 and 4), whereas in the $3p^5\epsilon p(^1D)$ and $3p^5\epsilon p(^1S)$ channels the $3p^4 4s^2$ and $3p^4 4s 5s$ states are also present. As was already mentioned, precise calculation of the resonance energies is a separate cumbersome problem. In more detail, in the present calculation the energy of the 4s electron is equal to $\epsilon_{4s} = -0.303$ Ry. When using the experimental value of the ionization potential $E_{3p^2}^{(i)} = 3.189$ Ry, the first terms in both denominators in Eq. (30) are vanishing at $\omega = 0.5 E_{3p^2}^{(i)} + \epsilon_{4s} = 17.57$ eV. This energy

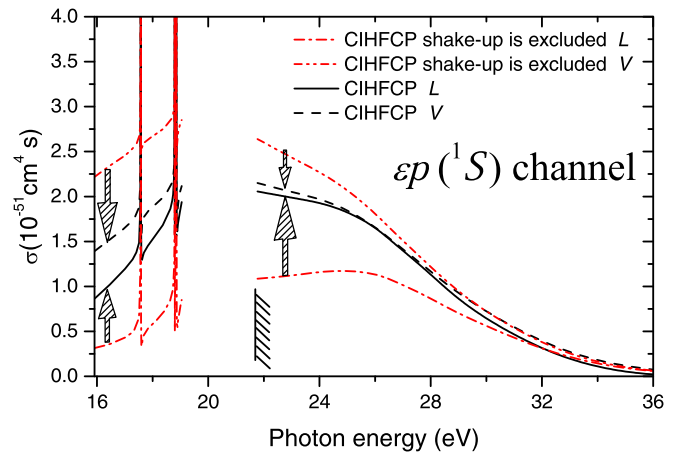


FIG. 6. Partial G2PICS for the transition to the $3p^5\epsilon p(^1S)$ channel, computed in length (L) and velocity (V) form for linearly polarized incoming radiation without (CIHFPC shake-up excluded) and with (CIHFPC) taking into account the shake-up correlation (IV). The two-photon $3p^4(^3P_2)$ ionization threshold is indicated by the hatched line.

corresponds to the position of the $3p^4 4s^2$ resonance in Fig. 5. The experimental energy of the $3p^4 4s^2$ resonance is at $\omega = 13.475$ eV [27]. The main reason for this discrepancy is the approximate (frozen-core) value of ϵ_{4s} .

In [9–11], a large influence of the intermediate-state shake-up (IV) correlation on the computed G2PICS was revealed, particularly on the $3p^5\epsilon p(^1S)$ partial cross section. In the ATI case, this influence is of similar size, as demonstrated in Fig. 6. Correlation (IV) influences both the real and the imaginary part of the transition amplitude and pulls together the $3p$ G2PICS computed in the length and velocity gauges.

Concluding this section, we demonstrate the effect of a successive inclusion of different correlations in the calculated total $3p$ shell G2PICS in Fig. 7. In Fig. 7(a), we compare the G2PICS computed in LOPT approximation with the cross sections obtained with taking into account correlations (II)–(VI). The drastic change of $\sigma(\omega)$ is obvious: a resonance structure appears below the two-photon $3p^4$ threshold, and a considerable enhancement of the above-threshold cross section together with a change of the shape of $\sigma(\omega)$ from a monotonic decrease to a curve with a broad maximum occurs. Those changes are mainly due to the electron-scattering correlation (VI), i.e., a $(3p \rightarrow \epsilon d)^2$ absorption of two exciting photons at the giant resonance with a subsequent Auger-type interaction $\epsilon d \epsilon d - 3p \epsilon f$. This mechanism should also influence the two-photon ATI of Xe in the range of its giant $4d \rightarrow \epsilon f$ resonance. An experimental proof by determining the two-photon G2PICS in Ar or Xe close to their respective $3p^4$ and $4d^8$ thresholds would be highly desirable.

In Fig. 7(b), the influence of the polarization of the atomic core by the photoelectron on the computed total cross section is presented. It results in a shift of the maximum of $\sigma(\omega)$ to lower photon energies and makes the humped curve more vivid. At the two-photon $3p^4(^3P_2)$ threshold the G2PICS increases by $\sim 33\%$.

In Fig. 7(c), the influence of the intrashell correlation on the dominating process (VI) and the effect of the correlational

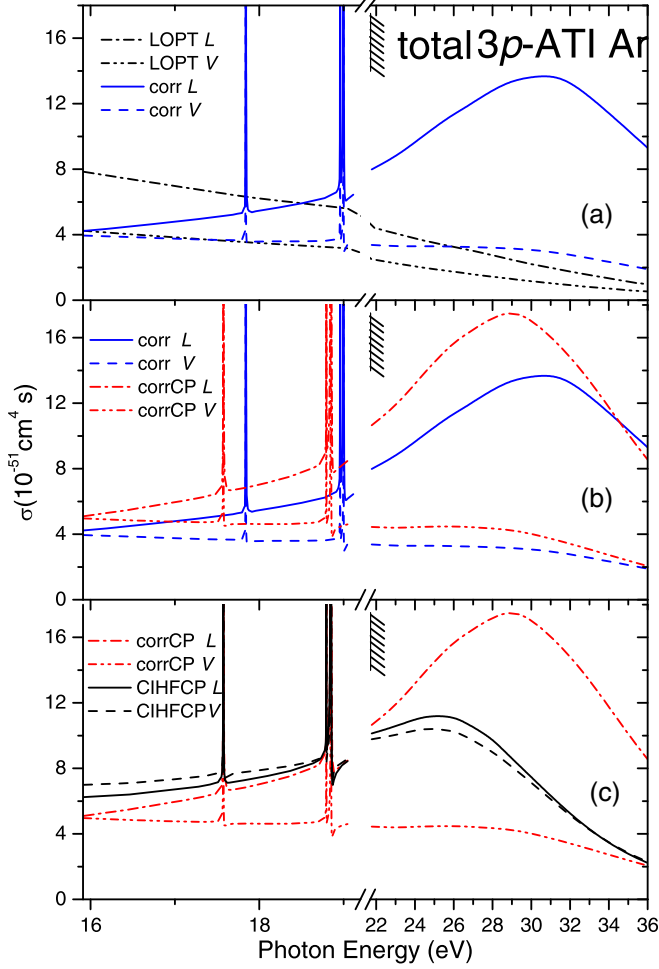


FIG. 7. The computed total $3p$ shell G2PICS in length (L) and velocity (V) form for linearly polarized incoming radiation. (a) LOPT approach and considering all the correlations (I)–(VI) (corr); (b) polarization of the atomic core by the photoelectron (corrCP) is included in addition to (a); (c) higher-order PT correlations (CIHFPC) are included in addition to (b). The two-photon $3p^4(^3P_2)$ ionization threshold is indicated by the hatched line.

decrease of the Coulomb interaction on the transitions (II)–(VI) is shown. These higher-order PT corrections bring the cross sections computed in length and velocity form in the considered photon-energy regions together.

IV. ANGULAR DISTRIBUTION OF PHOTOELECTRONS

The expression for the differential G2PICS is as follows:

$$\frac{d\sigma_q(\omega)}{d\Omega} = \frac{\sigma_q(\omega)}{4\pi} [1 + \beta_2^q(\omega)P_2(\cos\theta) + \beta_4^q(\omega)P_4(\cos\theta)], \quad (33)$$

where β_λ^q are angular distribution parameters for photoelectrons, P_λ are Legendre polynomials, and θ is the angle between the momentum of the photoelectron and the electric field vectors for linearly polarized incident radiation ($q = 0$) or between the momentum of photoelectron and the direction of propagation vectors of circularly polarized incoming radiation ($q = \pm 1$). The photoelectron angular distribution

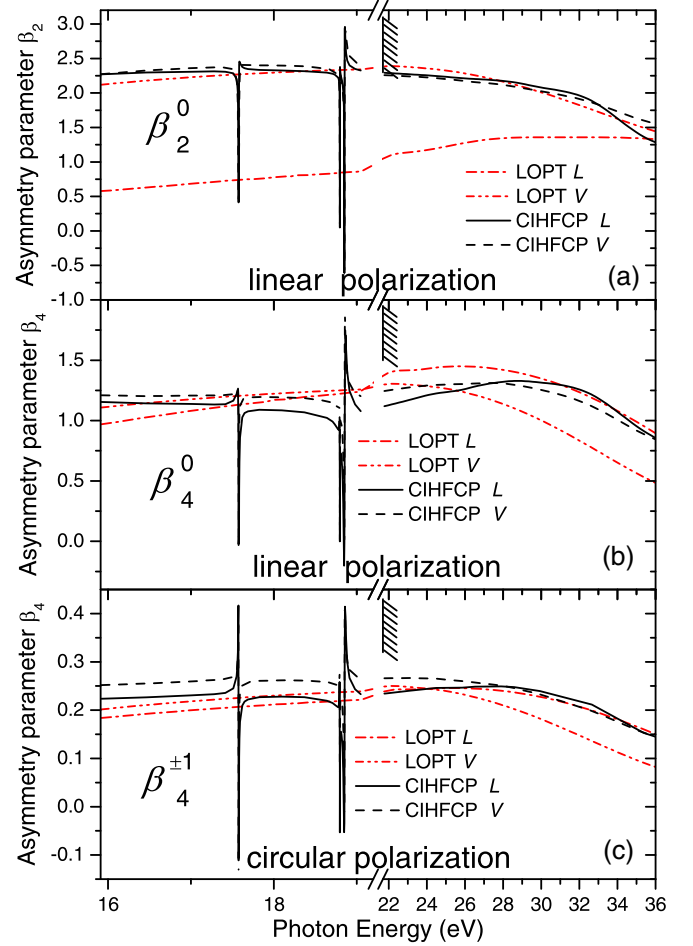


FIG. 8. Angular-distribution parameters β_λ^q for photoelectrons computed for the two-photon $3p$ ATI of Ar in length (L) and velocity (V) form in the LOPT approximation and with taking into account all the considered correlations (CIHFPC). The two-photon $3p^4(^3P_2)$ ionization threshold is indicated by the hatched line.

parameters β_λ^q are expressed via the transition amplitudes $T_{q,\omega}(L, \ell)$ discussed above. The corresponding expressions and numerical coefficients are reported in [10].

The results of the present calculation are depicted in Figs. 8(a)–8(c) for the β_2^0 , β_4^0 , and $\beta_4^{\pm 1}$ parameters, respectively. The β_2^0 and β_4^0 parameters describe the case of linearly polarized incoming radiation and $\beta_4^{\pm 1}$ is related to circularly polarized photons. The $\beta_2^{\pm 1}$ parameter is not presented in Fig. 8 because it is determined by the connection with $\beta_4^{\pm 1}$ via $\beta_2^{\pm 1} = -1 - \beta_4^{\pm 1}$ [10]. In all cases, taking into account many-electron correlations improves the agreement between length and velocity results.

The comparison between $\beta(\omega)$ computed in the LOPT approximation and with taking into account all the considered correlations exhibits a considerable change in $\beta(\omega)$ dependencies in the range where the doubly excited resonances are situated. The influence of many-electron correlations on $\beta(\omega)$ at $\omega \gtrsim 22$ eV is less pronounced than in the G2PICS case. To a large extent, this fact is connected with the prevalence of the $3p^5\epsilon f$ channel in the two-photon photoionization of Ar due to the influence of the $3p \rightarrow \epsilon d$ giant resonance.

V. CONCLUSIONS

In the present work, the two-photon ionization of the $3p$ shell of Ar in the above-threshold ionization (ATI) region was studied theoretically. For this purpose, we extended a noniterative correlation function (CF) technique developed earlier [10] to the case when both the CF and the final-state function are of continuum-type. We achieved an adequate degree of accuracy of the present calculations supported by good agreement between the results obtained in length and velocity form of the dipole transition operator.

The many-electron correlation, which can be treated as the $(3p \rightarrow \varepsilon d)^2$ absorption of the two exciting photons at giant resonance, plays a decisive role in two-photon ionization of Ar near the $3p^4$ threshold. Taking into account this correlation results in (i) an increase of the computed G2PICS by approximately three times and (ii) the appearance of resonance profiles in the energy range of the doubly excited $3p^4 n' \ell' n'' \ell''$ states ($15.76 < \omega < 21.69$ eV).

Taking into account all remaining single and double electron excitations in computing the transition amplitudes results in better agreement between G2PICS- L and G2PICS- V . Nevertheless, a three time difference between them in some partial photoionization channels still remains. This difference was removed after taking into account higher-order PT corrections. These corrections were included by (i) the polarization of the atomic core by the photoelectron, realized by incorporation of an *ab initio* polarization potential in the Hamilto-

nian; (ii) the effective correlational decrease of the Coulomb interaction, taken into account by computing respective reduction coefficients; and (iii) the intrashell correlations, taken into account via a technique described in [24]. Good agreement between length and velocity results for angular distribution parameters was also obtained after inclusion of the many-electron correlations described above.

Finally, our *ab initio* computation clarified that the two-photon above-threshold $3p$ ionization of Ar near the $3p^4$ threshold is almost entirely a collective-electron process. An experiment to benchmark the present prediction of the broad maximum in the G2PICS dependence above the two-photon $3p^4$ threshold and narrow resonances before this threshold is desirable.

ACKNOWLEDGMENTS

This work was supported by the Sonderforschungsbereich SFB1319 “Extreme light for sensing and driving molecular chirality” of the Deutsche Forschungsgemeinschaft (DFG). I.D.P., B.M.L., and V.L.S. would like to thank the Institute of Physics, University of Kassel for the hospitality. V.L.S. appreciates support from Southern Federal University within the inner Project No. 3.6105.2017/8.9. I.D.P. and B.M.L. appreciate support from Grant No. 16-02-00666A of the RFBR. We are grateful to A. Starace and L.-W. Pi for providing data from Fig. 2 of Ref. [12] in digital form. We are also grateful to A. Kramida providing us a reference with the experimental energy of the $3p^4 4s^2$ doubly excited state of argon.

-
- [1] W. Ackermann, G. Asova, V. Ayvazyan, and A. Azima, *Nat. Photon.* **1**, 336 (2007).
 - [2] T. Shintake, H. Tanaka, T. Hara, and T. Tanaka, *Nat. Photon.* **2**, 555 (2008).
 - [3] P. Emma, R. Akre, J. Arthur, and R. Bionta, *Nat. Photon.* **4**, 641 (2010).
 - [4] T. Ishikawa, H. Aoyagi, T. Asaka, and Y. Asano, *Nat. Photon.* **6**, 540 (2012).
 - [5] H.-S. Kang, C.-K. Min, and H. Heo, *Nat. Photon.* **11**, 708 (2017).
 - [6] M. S. Pindzola and H. P. Kelly, *Phys. Rev. A* **11**, 1543 (1975).
 - [7] A. F. Starace and T.-F. Jiang, *Phys. Rev. A* **36**, 1705 (1987).
 - [8] A. L’Huillier and G. Wendin, *Phys. Rev. A* **36**, 4747 (1987).
 - [9] C. Pan, B. Gao, and A. F. Starace, *Phys. Rev. A* **41**, 6271 (1990).
 - [10] I. D. Petrov, B. M. Lagutin, V. L. Sukhorukov, A. Knie, and A. Ehresmann, *Phys. Rev. A* **93**, 033408 (2016).
 - [11] B. M. Lagutin, I. D. Petrov, V. L. Sukhorukov, P. V. Demekhin, A. Knie, and A. Ehresmann, *Phys. Rev. A* **95**, 063414 (2017).
 - [12] L.-W. Pi and A. F. Starace, *Phys. Rev. A* **82**, 053414 (2010).
 - [13] F. Herman and S. Skillman, *Atomic Structure Calculations* (Prentice-Hall, Englewood Cliffs, NJ, 1963).
 - [14] F. Robicheaux and B. Gao, *Phys. Rev. A* **47**, 2904 (1993).
 - [15] A. R. Curtis, *Corpuscles and Radiation in Matter*, Vol. 11 of Royal Society Mathematical Tables, Coulomb Wave Functions (Cambridge University Press, Cambridge, 1964), pp. XXXV+209.
 - [16] M. Aymar and M. Crance, *J. Phys. B* **13**, L287 (1980).
 - [17] B. Gao and A. F. Starace, *Comput. Phys.* **1**, 70 (1987).
 - [18] T. Åberg and G. Howat, *Corpuscles and Radiation in Matter*, Vol. 31 of Encyclopedia of Physics, Theory of the Auger Effect (Springer, Berlin, 1982), pp. 469–619.
 - [19] A. Burgess, *Proc. Phys. Soc.* **81**, 442 (1963).
 - [20] A. Kramida, Y. Ralchenko, J. Reader, and NIST ASD Team, *NIST Atomic Spectra Database (version 5.2) [online]* (National Institute of Standards and Technology, Gaithersburg, MD, 2014).
 - [21] V. Sukhorukov, B. Lagutin, H. Schmoranzer, I. Petrov, and K.-H. Schartner, *Phys. Lett. A* **169**, 445 (1992).
 - [22] V. L. Sukhorukov, B. M. Lagutin, I. D. Petrov, S. V. Lavrentiev, H. Schmoranzer, and K. H. Schartner, *J. Electron Spectrosc. Relat. Phenom.* **68**, 255 (1994).
 - [23] S. Kammer, K.-H. Schartner, S. Mickat, R. Schill, A. Ehresmann, L. Werner, S. Klumpp, H. Schmoranzer, I. D. Petrov, P. V. Demekhin, and V. L. Sukhorukov, *J. Phys. B* **39**, 2757 (2006).
 - [24] M. Amusia and N. Cherepkov, *Many-electron Correlations in Scattering Processes*, Vol. 5 of Case Studies in Atomic Physics (North-Holland, Amsterdam, 1975), pp. 49–179.
 - [25] I. D. Petrov, V. L. Sukhorukov, and H. Hotop, *J. Phys. B* **32**, 973 (1999).
 - [26] I. D. Petrov, V. L. Sukhorukov, and H. Hotop, *J. Phys. B* **36**, 119 (2003).
 - [27] K. Jorgensen, N. Andersen, and J. O. Olsen, *J. Phys. B* **11**, 3951 (1978).